PDI-functionalised glass beads: efficient, metal-free heterogeneous photocatalysts suitable for flow photochemistry

Hamza Ali[a], Karen Robertson*[b], Ifty Ahmed[b], and Anabel E. Lanterna*[a]

[a] School of Chemistry, University of Nottingham, University Park, Nottingham, NG7 2RD, UK

[b] Advanced Materials Research Group, Faculty of Engineering, University of Nottingham, University Park, Nottingham, NG7 2RD, UK

Abstract: Perylene diimides (PDI) have an extraordinary ability to activate both energy and electron transfer process upon light excitation, however, their extremely low solubility has hindered their wide use as photocatalysts. Here, we show a series of supports developed to anchor PDI and to enable its use as a heterogeneous photocatalyst in diverse reactor set-ups. Inert, easy-to-handle, glass microspheres of various morphological and chemical properties were chemically functionalised with PDI to form an inorganic-organic hybrid material. Using the photo-oxidation of n-butyl sulfide as a benchmark reaction for the synthesis of sulfoxides, we show that immobilised PDI are highly active, outperforming reported homogeneous photosensitisers, and capable of reuse in both batch and flow reactors. Transferring the process from batch to flow resulted in a 10-fold reduction in irradiation time and an increase in the space-time-yield by a factor of 10 (0.04 vs 0.38 $mmol^{-1}$ h^{-1} mL^{-1} batch vs flow). This work combines the remarkable photocatalytic properties of PDI with inert, easy to handle glass beads, producing hybrid materials that are reusable and can be adapted for performing heterogeneous photocatalysis in a range of scalable photochemical reactors.

Introduction

Photocatalysis is increasingly being used as a tool for sustainable synthesis of fine chemicals and pharmaceuticals,[1-3] however, large-scale adoption is limited due to design of suitable reactors and processes. As the absorbance of light by the reaction media is a function of the reactor path length, the amount of light at the centre of a large reactor is significantly lower than that at its surface, especially for strongly coloured solutions. Increasing the intensity of light is not a tenable solution as this over-irradiates the edge of the reactor, potentially leading to overreaction, decomposition of product and fouling. Flow photoreactors help overcome these limitations through reduction of the path length between the light source and reaction mixture using narrow channels.[4-7] Continuous flow systems also provide better heat and mass transfer, usually making the process safer, faster, and allow for fine control of factors underpinning product quality such as residence time and reagent stoichiometry.[8-9] Thus, due to the relatively smaller reaction volumes compared with batch reactors, flow systems allow for better control of reaction temperature and mixing of reagents, avoiding side reactions and leading to higher yields, thereby reducing waste generation associated with downstream processing (i.e., separation).[10-12] Flow reactors are inherently compatible with photocatalytic processes and have found use in the pharmaceutical industry due to their small footprint, potential for automation and enhanced sustainability credentials.[13] However, most photocatalytic processes employ homogeneous photocatalysts, which are often used once and require separation from the product. Heterogeneous photocatalysts offer the potential for reusability and ease of removal from the reaction stream, but their use in flow systems remains a challenge due to the inherent difficulty of flowing solids through narrow channels causing issues such as clogging and poor flow dynamics.[14-16] As such, fixed-bed reactors could be more suitable as the catalyst sits in the tube while the reagents are flown through.[17] Nevertheless, careful design of materials is needed to effectively use heterogeneous photocatalysts in fixed-bed reactors: large catalyst particle size leads to low surface area-to-volume ratios, limiting catalyst concentrations; however, the use of finer particles increases the back pressure, introducing process safety concerns (Figure 1).

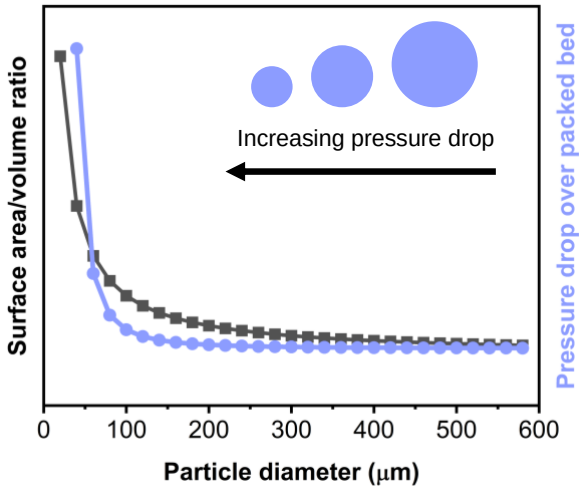

Figure 1: Increase in particle surface area/volume ratio (SA/vol) as well as pressure drop as a function of particle diameter, d. Increase in SA/vol is proportional to 1/d, increase in pressure drop is proportional to ($1/d^2$ + 1/d).

There are various published designs for flow photoreactors including immersion wells[18], FEP tubular reactors[4], parallel plate reactors[19], in addition to more exotic reactor geometries such as spinning disk[20] and vortex reactors.[8] A commonly used design is a packed-bed reactor, where the photocatalyst is in a transparent housing, usually glass or a transparent polymer tubing (e.g. FEP). Packed-bed reactors are a form of fixed-bed reactor wherein the catalyst is confined within a given region, and both gaseous and/or liquid reactants can be passed over the catalytic zone, with products exiting the end. The benefits of this approach include ease-of-assembly, effective mixing between phases, and immobilisation of the catalyst leading to simpler separation, avoiding wasteful catalyst removal steps.[21] This approach also opens the possibility for facile real-time reaction feedback using imaging or spectroscopy based in-line analysis making these reactors suitable for implementation into self-optimising systems, or as part of multi-step sequential flow reactions [22-23]A common strategy to prepare heterogeneous photocatalysts relies on anchoring homogeneous photocatalysts (e.g. tris(bipyridine) ruthenium(II) chloride ($Ru(bpy)_3Cl_2$)) onto silica-based supports such as glass wool[24], glass beads,[25] silica gel[26] and mesoporous silica[27]. Whilst simple, this heterogenisation approach often relies on the electrostatic interactions between the physisorbed catalytic

species and the support, frequently resulting in catalyst desorption into the solution during use,[28] making such materials unsuitable for flow chemistry applications. Pre-activation of the support can provide stronger anchoring points, but the formation of strong covalent bonds between the photocatalyst and support is necessary to prepare a durable, long-lived, heterogeneous catalyst.[29-31] Using this strategy, we have previously pioneered the use of inexpensive and widely available materials such as glass wool as a support to run heterogeneous photocatalytic processes: examples show organometallic complex[31] or metal nanoparticle catalysts,[24] used in batch and flow applications.[32] Additionally, organic dyes supported on silicon-based materials have been shown to be a powerful, low-cost, sustainable alternative to organometallic compounds offering a greener pathway for heterogeneous photocatalysis.[33] This includes perylene dyes, which show great photostability and can be used in different photoredox processes or as photosensitizers.[34-37] Perylene diimides (PDI) and its derivatives are known singlet oxygen ($^1O_2$) photosensitisers, however, their use in photocatalysis has been hindered by their low solubility in common organic solvents. Attempts to use them in heterogeneous phase have been shown in the past[30] including uses in combination with well-known inorganic photocatalysts such as TiO_2.[38] Nevertheless, the small particle size of commonly used supports such as mesoporous silica (e.g. SBA-15, MCM-41) presents issues when used with flow systems, as described above.

In this study, we are trialling use of solid (dense) glass beads and uniquely highly porous glass beads as catalysts supports for creating a PDI-based photocatalyst in flow. As opposed to glass wool, glass beads provide ease for packing and greater mechanical stability. Glass beads have previously been used as refractive components to increase light penetration and as supports of photocatalysts such as TiO_2 and fluorescein polymers.[25, 39] Furthermore, they also find use as static mixers within flow chemistry systems to improve mass transfer in multi-phasic mixtures.[40] The use of glass beads allows for repeatable packing into tubular reactions, and their spherical shape permits ease of loading into flow reactors (*via* a slurry). Herein, we explore a series of supports based on glass beads that have been easily functionalised with perylene-based photocatalysts and hence used for the oxidation of *n*-butyl sulfide in batch and flow systems. The supported PDI catalyst performs well with high conversion and excellent selectivity in the synthesis of *n*-butyl sulfoxide. The nature of the supporting materials (i.e., borosilicate beads and phosphate based glass microspheres) exhibit morphological and chemical properties that make them reusable, easy to separate, and compatible with fixed-bed flow reactors (ease of loading and unpacking), providing an excellent platform for sustainable and scalable aerobic oxidative processes in continuous flow.

Results and Discussions

The use of solid supported PDI photocatalysts requires supports that are compatible with lab scale reactors and easily adaptable to flow systems that can facilitate large scale production. Two photoreactors are considered for testing the materials (Fig. S1-S2): a) A thin-film rotary photoreactor, modelled after the 'PhotoVap' by Poliakoff and George[41] and b) a fixed-bed FEP flow reactor.[2] The thin-film photoreactor is used in batch operation to complete solid-gas-liquid photochemical studies under different gaseous environments. The rotary nature of this reactor allows for mixing without the need for a stirrer bar or impeller, minimising the mechanical stress experienced by the solid phase and therefore detachment of the superficial dye layer. The second, a fixed-bed reactor, presents several advantages for using heterogeneous materials in flow, but also some limitations regarding particle size, as small particle sizes can increase the back pressure of the system also limiting the appropriate length of the reactor. Operating at conditions close to the working pressure limit also has implications on process safety, particularly when using flammable organic solvents with gaseous oxygen.[42] Therefore, we decided to evaluate supports (table 1) with different sizes and morphologies, from commercial glass beads (GB1 and GB2, entries i-ii) to porous phosphate-glass microspheres (PGB1, PGB2, and PGB3; entries iii-v) manufactured in-house at the University of Nottingham. The materials were selected to provide varied surface area for catalyst loading while reducing pressure drops when used in fixed-bed flow reactors.[43-46] All materials were characterised by scanning electron microscopy (SEM, Fig. 2 and Fig. S3-S4) and N_2 adsorption analysis (Fig. S5-S6) to determine morphology and surface area, respectively.

Table 1: Properties of the catalyst support materials used in this work.

Entry	Label	Composition	Morphology	Particle size (μm)[a]	Surface area ($m^2\ g^{-1}$)[b]
i	GB1	Borosilicate glass[c]	Solid microspheres	133 – 215	2.39
ii	GB2	Borosilicate glass[c]	Solid microspheres	424 – 807	1.23
iii	PGB1	Phosphate glass [d,e]	Porous microspheres	65 – 124	1.38
iv	PGB2	Phosphate glass [d,e]	Porous microspheres	115 – 206	2.25
v	PGB3	Ti-doped phosphate glass[d,e]	Porous microspheres	118 – 211	2.56

[a] Determined by SEM imaging analysis. [b] Determined using N_2 gas adsorption experiments using Brunauer-Emmett-Teller (BET) model. [c] Commercially available. [d] Materials synthesised following reported methods.[47] [e] Materials are soluble at low pH aqueous solutions.

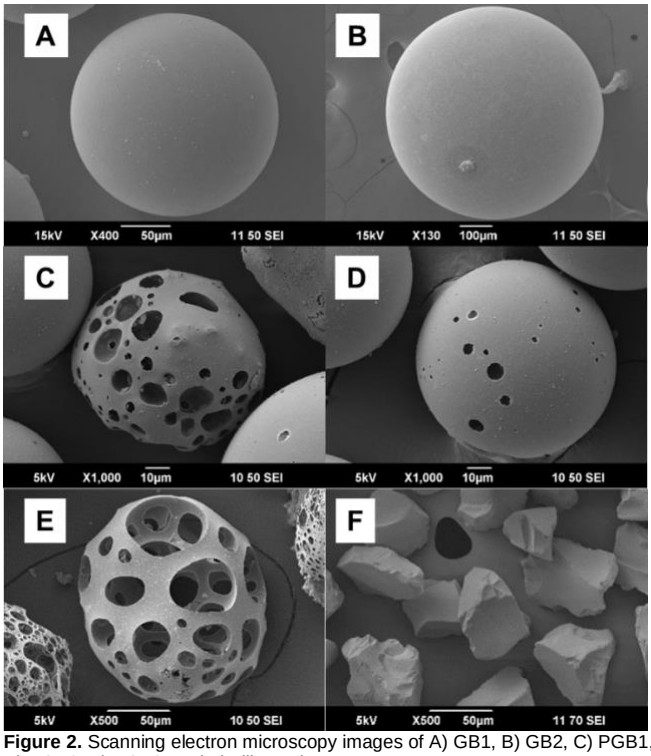

Figure 2. Scanning electron microscopy images of A) GB1, B) GB2, C) PGB1, D) PGB2, E) PGB3, and F) silica gel.

To test the materials suitability for a fixed-bed reactor (Fig. S2), we designed a series of pressure drop experiments to determine the correlation between particle morphology and pressure generation under fluid flow conditions. The pressure drop per unit length (ΔP/L) across a fixed bed of length L, as described by the Ergun equation,[48] is a function of the physical properties of the fluid, the reactor dimensions, the particle size and the bed porosity as well as the fluid properties of the components passing through the packed bed (i.e. fluid viscosity, further details in SI). Generally, ΔP/L increases with decreasing particle size and increasing packing density. Thus, the ideal support should be capable of being deployed in a fixed-bed reactor without being too fine to generate high pressures, yet small enough to maintain a high surface area-to-volume ratio for efficient catalyst loading. Figure 3 shows the pressure drops experienced in fixed-bed reactors related to particle size, porosity, and reactor dimensions. As expected, the support morphology plays a crucial role in the pressure drop experienced by the system, thus, spherical particles show significant lower pressure drops than amorphous silica gel (Fig. 3A), which is expected giving the combination of significantly different particle size as well as the angular shape of silica. A larger void fraction is expected to result in a lower pressure drop. Pressure drops are reduced when using porous particles, potentially allowing for longer reactors before nearing the working pressure limit for the tubing. Fig. 3B shows the particle size also affects the pressure drop as expected, with lower particle sizes generating higher pressures. Overall, the results show both solid and porous beads would allow the use of a ~10 m long reactor while still working below the maximum safe working pressure (< 300 psi) demonstrating the ease of scalability of this platform.

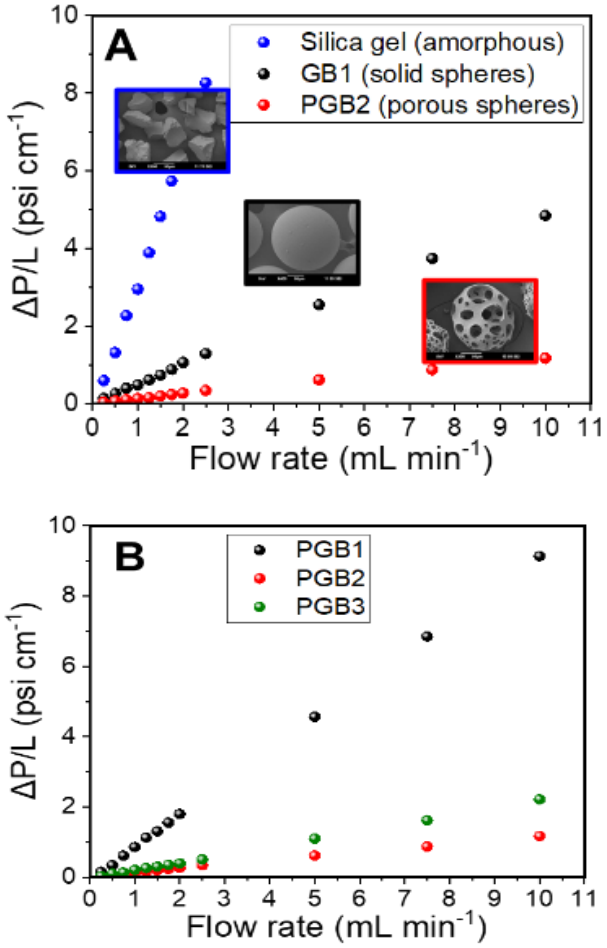

Figure 3. Back pressure experienced as a function of IPA flow rate over a fixed-bed reactor (ID = 0.085 in) for amorphous silica gel, GB1, PGB1, PGB2 and PGB3. The plots compare particle morphology and particle porosity (A), and porous particle size (D). RSD < 1 %.

Next, we tested the materials' resistance to withstand the reactions conditions during catalyst loading and to ensure appropriate catalyst lifetime. As catalyst loading requires pre-activation of the particles under either acid or basic conditions, the materials were subjected to these conditions and their chemical resistance was visually evaluated. In the case of the solid borosilicate glass beads (GB1, GB2), the surface activation could be completed with Piranha solution resulting in sticky, hydrophilic beads due to the increased concentration of surface Si-OH groups. As the same conditions lead to complete disintegration of the porous beads (PGB1, PGB2 and PGB3), alternative basic conditions were used to activate these materials (See ESI).

PDI-grafted glass beads

The materials showing the most promising mechanical and chemical properties, this is, reduced pressure drops, resistance to activation conditions, and strength under spinning conditions (not shown), were selected to anchor the PDI photocatalyst, i.e., GB1 and PGB3. For this we use a covalent cross-linker, APTES (3-aminopropyltriethoxysilane), an aminosilane of benign nature and low cost (see ESI for details). APTES can form strong bonds between silica surfaces through the formation of Si-O-Si linkages allowing them to bind to a range of photosensitisers[30-31]. Silanisation of activated silica-based materials is an effective approach for subsequent modification. The formation of a surface layer of a covalently anchored PDI units is expected to give a strongly bound photocatalyst that retains its homogeneous phase

catalytic properties allowing for the activation of both energy transfer and SET (single-electron transfer) processes. The resulting hybrid material (PDI@support) shows a strong pink colour suggesting effective loading of the PDI onto the glass beads. The optical characterisation shown in Fig. S8 is representative of the materials obtained using this protocol. The theoretical amount of PDI distributed across the surface of the glass bead was estimated assuming glass bead's geometry and formation of a PDI monolayer (Table S1). Experimental values were determined via PDI detachment upon base-catalysed hydrolysis[49] (see ESI) followed by analysis of the liberated dye using UV/vis spectroscopic analysis. This led to experimental loadings of 0.195 µmol g^{-1} for PDI-GB1 which is comparable to the theoretical value of 0.15 µmol g^{-1}. The differences between predicted and measured loadings are likely due to deviations from theoretical assumptions such as microsphere size and the formation of a monolayer of PDI.

Photocatalytic process: batch conditions

PDI compounds have previously been used for a wide variety of organic transformations such as the reduction of aryl halides, iodoperfluorination of alkenes and the aerobic oxidation of sulfides.[34, 50] Here, we used the oxidation of *n*-butyl sulfide (Table 2) as a model reaction to test the catalytic properties of the prepared materials. The corresponding sulfoxide is commonly found within pharmaceuticals (e.g. omeprazole and sulindac [51]), agrochemicals and polymers. Sulfoxidation strategies have been reported including the use of photocatalysts such as anthraquinone and thioxanthone.[52-54] PDI compounds bearing isopropylbenzene end groups have been used in homogeneous phase for the photochemical sulfoxidation of *n*-butyl sulfide with high conversions and selectivity, but no attempt was made to recover the photocatalyst to test reusability of the material.[35] The activity of the PDI-beads was first tested in batch conditions using the thin film rotary photoreactor (Fig. S1). As shown in Table 2, the reaction proceeds to completion in less than 2 h when using MeCN or MeOH as solvents. The use of EtOH, a less toxic solvent, shows slightly lower reaction kinetics, despite theoretically having the greatest O_2 solubility.[55] Nevertheless, complete conversion of the sulfide is achieved in 2.5 h with complete selectivity towards the sulfoxide. The presence of *n*-butyl sulfone was not detectable by GC or ^{1}H NMR. Control experiments (Table 3) show the reaction cannot proceed in the absence of catalyst or in the dark (entries ii, iii). Also, both O_2-enrichment of the solvent as well as maintaining an O_2 environment within the flask were beneficial to increasing yield demonstrating the importance of maximising O_2 availability for the sulfoxidation to proceed. Kinetic studies show zero order with respect to the concentration of substrate across the range explored (Fig. 4A). Thus, the rate of the photo-oxidation is limited by the generation of reactive oxygen species (ROS), which depends on light intensity, oxygen and photocatalyst concentration. Fig. 4B shows the reaction rate increases linearly with light intensity. As commonly found in both homogeneous and heterogeneous photocatalytic systems, the reaction rate tends to increase linearly with photocatalyst concentration (Fig. 4C), due to enhanced light absorption, till reaching a plateau at peak light absorption.

Table 2. Solvent effect on the photocatalytic oxidation of *n*-butyl sulfide under batch conditions.[a]

Entry	Solvent	Time (h)	Conversion (%)	Yield (%)
1	MeCN	1	72	68
2	MeCN	2	>99	>99
3	MeOH	1	68	63
4	MeOH	2	>99	>99
5	EtOH	1	45	40
6	EtOH	2	70	66
7	EtOH	2.5	>99	>99

[a]Reaction conditions: 0.5 mmol *n*-butyl sulfide, 2 g PDI-GB1 (0.03 mol %), 5 mL O_2-enriched solvent, O_2 atmosphere. LED: 456 nm. Irradiance: 0.58 W cm^{-2}. Reaction followed by gas chromatography (GC) using 1,3,5-trimethoxybenzene as an external standard.

Table 3. Oxygen concentration effect on the photocatalytic oxidation of *n*-butyl sulfide under batch conditions.[a]

Entry	Change of conditions	Conv (%)	Yield (%)
i	None	>99	>99
ii	Dark	Trace	0
iii	No catalyst	Trace	0
iv	O_2-enrichment, Air atm	28	25
v	No O_2-enrichment, O_2 atm	51	49
vi	O_2-enrichment. Ar atm	11	8
vii	Ar degassing, Ar atm	Trace	0
viii	Ar degassing, O_2 atm	45	43

[a]Reaction conditions: 0.5 mmol *n*-butyl sulfide, 2 g PDI-GB1 (0.03 mol %), 5 mL EtOH, 2 h irradiation. LED: 456 nm. Irradiance: 0.58 W cm^{-2}. Reaction followed using gas chromatography (GC) with 1,3,5-trimethoxybenzene as an external standard.

To further demonstrate the applicability of these materials, the sulfoxidation of *n*-butyl sulfide was carried out at gram-scale. We observed a 20-fold increase to 10 mmol (~1.5 g) of n-butyl sulfide was quantitatively converted to the corresponding sulfoxide in 16 h. This is comparable to similar aerobic oxidations of sulfides using homogeneous photosensitisers in batch. [54] The beads were recovered and re-used without loss of activity (Fig. 4D). Additionally, the catalyst was reused at least 5 times in batch conditions with cumulative turnover numbers (TONs) nearing 16,000 after the 5th run. The turnover frequency (TOF) remains largely unchanged across the five catalytic cycles, with a slight decrease from 1,111 to 1,107 h^{-1} by the 5th use of the same material, respectively. These experiments led to detachment of dye from the support (see Fig. S10), potentially due to remnant PDI physisorbed via π-π bonding between PDI units. Furthermore, the shear mechanical forces experienced by the bead during rotation is expected to lead to attrition between particles. Nevertheless,

the amount of PDI loss is estimated to roughly 1% of the total PDI loading, which did not affect the overall activity of the catalyst. Fortunately, the catalyst loss can be circumvented under flow conditions as shown below (Fig. S10).

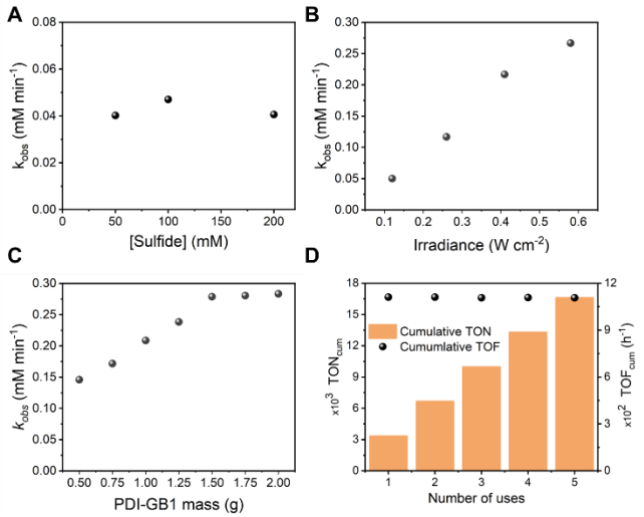

Figure 4. Kinetic studies to determine the order of reaction with respect to A) *n*-butyl sulfide concentration (Irradiance: 0.12 W cm^{-2}), (B) light intensity and (C) photocatalyst loading (MeOH instead of EtOH). (D) Reusability of PDI-GB1. Reaction conditions: 0.5 mmol *n*-butyl sulfide, 2 g PDI-GB1, 5 mL O_2–enriched EtOH, O_2 atmosphere. LED: 456 nm (typically 0.58 W cm^{-2}). Reaction followed by gas chromatography (GC) using 1,3,5-trimethoxybenzene as an external standard.

Photocatalytic process: flow conditions

The PDI-beads materials were tested in a fixed-bed flow reactor (FEP tubing, Fig. S1 – S2). The reactor was illuminated from the side using a 459 nm LED (1.2 W cm^{-2}). The dosing of liquid reagents at a fixed flow rate, Q, was controlled by a syringe pump allowing for precise delivery of substrate. The liquid stream was connected to a T-mixer with a flow of O_2 gas (set using a mass flow controller) to form a segmented flow of alternating liquid-gas slugs. This flow pattern leads to highly efficient micro mixing between the two phases due to the presence of counter-rotating vortices at the phase interface (Taylor vortices).[15] The segmented flow pattern was maintained after exiting the reactor albeit with an increase in both the size of the liquid slugs as well as the spacing between consecutive slugs, likely due to the presence of the fixed-bed of beads resulting in axial dispersion of fluid flow and coalescence of segments.

The reaction proceeded with high efficiency across a range of process conditions including different flow rates and substrate concentrations (Table 4). The nature of the support material affected the reaction outcome significantly, with solid glass beads producing the sulfoxide product quantitatively (entries i-ii). Porous phosphate beads allow for sulfone formation, potentially due to increase local concentration of oxygen and reagent inside the pores (entries iii-iv).

In order to increase productivity, longer reactor lengths were used. The concentration of *n*-butyl sulfide could be increased from 0.05 to 0.075 M leading to an increase in hourly productivity from 1.15 to 1.71 mmol h^{-1} (entries v-vi). An attempt was made to maintain the same residence time (RT: 11 min) and further increase the reaction concentration to 0.1 M but this led to a poorer conversion and yield of 60% (entry vii). Nevertheless, doubling the residence time to 23 min achieved full conversion of the starting material and quantitative conversion into *n*-butyl sulfoxide but the reduced flow rate decreased the hourly productivity to 1.19 mmol h^{-1} (entry viii). The effect of flow rate was explored further, and it was possible to maintain a comparable yield with an RT of 15 min increasing the hourly productivity to 1.76 mmol h^{-1} (6.9 g day^{-1}, entry ix). Remarkably, no PDI leaching was detected under flow conditions, as opposed to the loss of PDI experienced in the rotary thin film reactor (see Fig. S10). This suggests that under flow conditions the material experiences lower shear forces than in batch, resulting in low mechanical stress and undetectable catalyst loss. The back pressure generated during fluid flow at process conditions was typically less than 10 – 15 psi which provides confidence in the scale-up of this reactor through either a longer coil or a wider diameter tubing. Furthermore, none of the typical issues experienced when using heterogeneous materials in flow such as blocking, and clogging were experienced due to immobilization of the catalytic phase inside the packed bed.

Table 4: Flow chemistry experiments completed in fixed-bed photochemical reactor.

Entry[a]	Catalyst	[Sulfide] (mM)	Q (mL min^{-1})	RT (min)	Conversion (%)	Yield (%)	Productivity	
							mmol h^{-1}	mmol h^{-1} L^{-1}
i	PDI-GB1	25	0.025	5	78	74	0.03	185
ii	PDI-GB1	25	0.010	10	>99	96	0.01	96
iii[b]	PDI-PGB3	25	0.025	5	60	40	0.02	140
iv[b]	PDI-PGB3	25	0.010	10	67	52	0.01	65
v	PDI-GB1	50	0.4	11	>99	96	1.15	640
vi	PDI-GB1	75	0.4	11	>99	95	1.71	950
vii	PDI-GB1	100	0.4	11	68	60	1.44	800
viii	PDI-GB1	100	0.2	23	>99	>99	1.19	660
ix	PDI-GB1	100	0.3	15	>99	98	1.76	980

Reaction conditions: *n*-butyl sulfide, O_2-enriched EtOH. LED: 456 nm. Irradiance: 1.2 W cm^{-2}. Reaction followed using gas chromatography (GC) with 1,3,5-trimethoxybenzene as an external standard. [a] Reactor length: 10 cm (entries i-iv), 5 cm (entries *v-vi*), and 120 cm (entries *vii-xi*). [b]Yield drops are the result of ~20% sulfone formation. Q: liquid flow rate, RT: residence time. Productivity (mmol h^{-1}) = concentration (M) x flow rate (mL min^{-1}) x yield x 60 $min h^{-1}$. Space-time yield (STY, mmol h^{-1} L^{-1}) = productivity / reactor volume.

Conclusions

We demonstrated the use of silane-ended perylene diimide for the creation of a heterogeneous photocatalyst suitable for continuous flow applications. Its photocatalytic properties were tested through the generation of reactive oxygen species for the oxidation of *n*-butyl sulfide as a benchmark reaction. The reaction proceeded with fast kinetics in batch providing confidence for using PDI-beads in flow reactors. A fixed-bed FEP flow reactor was developed to use both supports, solid glass beads (GB1) as well as porous phosphate-glass beads (PGB3), in a continuous flow gas-liquid system. The nature of the support affects the reaction productivity, with porous beads providing a route to the synthesis of the overoxidised product, sulfone, whereas the solid beads produced sulfoxide quantitatively. It was possible to achieve hourly productivities of 1.76 mmol h^{-1} (~7 g day^{-1}) and space-time yields of up to 980 mmol h^{-1} L^{-1}. By immobilising a thermally and photochemically durable photocatalyst, it is possible to achieve TONs of >16,000. The use of supported-PDI in a simple fixed-bed photochemical reactor housed in FEP tubing eliminates the need for a costly catalyst removal stage. The ease-of-use, simple assembly and scalability of this reactor demonstrates the applicability of this system for fine chemical synthesis using visible light.

Experimental Section

Materials and methods

Commercially-available, solid, glass beads (150 – 212 µm, 500 – 750 µm) as well as a range of porous, phosphate-based, glass microspheres were used as supports. Hydrogen peroxide (12%) and sulfuric acid (S.G.1.8) were used to prepare piranha solution for support surface activation. Perylene-3,4,9,10-tetracarboxylic dianhydride (PTCDA) and 3-aminopropyltriethoxysilane (APTES) were used to prepare the PDI. Analytical standard *n*-butyl sulfide, *n*-butyl sulfoxide, *n*-butyl sulfone, 1,3,5-trimethoxybenzene were purchased from Sigma-Aldrich. FEP tubing was purchased from Cole-Parmer. Fittings for the flow reactor were obtained from Swagelok and Cole-Parmer. LED lamps from Kessil Lighting and University of Nottingham workshops.

Synthetic procedures

Synthesis of PDI

PDI was synthesised via a reported literature method[30] with slight modifications. Briefly, PTCDA (2 g) was purged with N_2 in a round bottom flask. APTES (4 mL, ~4 eq.) was injected into the flask and the resulting mixture was stirred for 20 h under an N_2 atmosphere in the dark at 150 °C. The resulting red solid was ground to a fine powder and transferred to a Soxhlet system for extraction with petroleum ether for 7 days to remove unreacted APTES, followed by extraction with acetone for 2 days to remove residual PTCDA. Acetone was used to recover the solid and subsequently removed under reduced pressure to afford the PDI as a dark red powder.

Activation of support

Briefly, glass beads were activated using Piranha solution (3:1 H_2SO_4:H_2O_2). The beads were washed with DI water and dried in an oven at 80 °C for 2 h. For porous beads (PGB1-3), a concentrated base etch (10 M, methanolic) was used at room temperature.

Synthesis of PDI-beads

PDI was immobilised onto silica supports using a standard protocol (Scheme S2). Depending on the nature of the support, one of two activation routes was taken (above). The activated beads were immediately transferred into a round-bottom flask with 50 mL anhydrous toluene, 0.3 g PDI and refluxed overnight. The PDI-beads were washed toluene (x2), acetone (x2) and methanol to remove unreacted PDI and transferred to a Soxhlet system for extraction with acetone for 2 days.

Photocatalytic procedures

Batch conditions

The batch photochemical oxidation of *n*-butyl sulfide was carried out in a thin-film rotary photoreactor (Fig. S1). Typically, a 50 mL round bottom flask was charged with 0.5 mmol *n*-butyl sulfide, 5 mL O_2-enriched solvent and 2 g PDI-beads. The flask was connected to the evaporator under an oxygen environment. Rotation speed was set to simultaneously suspend the glass beads as well as create a thin film to maximise the contact between gas-liquid-solid phases. The flask was partly submerged in water bath (to maintain a constant reaction temperature between 18 – 20 °C) and irradiated using an LED lamp. For the gram scale experiment, the reaction was completed in a 250 mL round bottom flask with 15 g PDI-beads in 10 mL oxygen-enriched EtOH, irradiating with blue LED (0.58 W cm^{-2}) for 16 h. Reactions were followed by gas chromatography (GC) using 1,3,5-trimethoxybenzene as an external standard.

Flow conditions

Flow photochemistry was tested in a fixed-bed FEP flow reactor (Fig. S1 – S2). A syringe was loaded with a solution of *n*-butyl sulfide in O_2-enriched EtOH. Liquid flow into the system was controlled using a syringe pump and was combined with a stream of O_2 using a T-mixer. Gas flow was set either at the cylinder regulator (1 bar) or metered into the reactor using a mass flow controller (Alicat Scientific, Inc.) The two fluids streams were combined in a T-mixer until a segmented flow pattern was achieved. The reactor was irradiated using a blue LED lamp and samples for yield and conversion determination were taken after 3 reactor volumes to measure steady state concentration.

Characterisation

Gas chromatography was completed on a Thermo Fisher 1310 system. FT-IR spectra were acquired using a Bruker Alpha IR spectrometer with an ATR accessory. A JEOL 6490LV scanning electron microscope was used to evaluate the size and morphological properties of solid-state materials used in this study. N_2 adsorption isotherm data was acquired using a Micromeritics 3Flex adsorption analyser. Surface area was approximated using the Brunauer-Emmett-Teller (BET) approximation. Absorption properties of the synthesised materials were evaluated using an Agilent Cary 5000 spectrophotometer using a DRA-1800 (PMT/InGaAs) diffuse reflectance accessory. Absorption and emission spectroscopies were obtained using a Tecan Infinite 200 PRO plate reader. Solid state photoluminescence spectra were acquired using an Edinburgh Instruments FLS980 system using a Xe source lamp and a 590 nm cut-off filter.

Further experimental details and data are provided in the accompanied Supporting Information.

Acknowledgements

We thank the Engineering and Physical Sciences Research Council (EPSRC) and SFI Centre for Doctoral Training in Sustainable Chemistry, Astra Zeneca and The Royal Society for funding this research. We thank the Nanoscale and Microscale Research Centre (nmRC) and the University of Nottingham for access to instrumentation, Mr Mark Guyler for valuable technical support, Prof. Robert Mokaya and Mr Nawaf Albeladi for support with and training in gas adsorption analysis.

Keywords: heterogeneous photocatalysis • sulfoxidation • continuous flow • process intensification

Corresponding authors:

AEL: anabel.lanterna@nottingham.ac.uk

KR: karen.robertson@nottingham.ac.uk

References

1. A perspective on continuous flow chemistry in the pharmaceutical industry, Baumann, M.; Moody, T. S.; Smyth, M.; Wharry, S., *Org. Process Res. Dev.* **2020,** 24(10), 1802.
2. A practical flow reactor for continuous organic photochemistry, Hook, B. D. A.; Dohle, W.; Hirst, P. R.; Pickworth, M.; Berry, M. B.; Booker-Milburn, K. I., *J. Org. Chem.* **2005,** 70(19), 7558.
3. Photocatalysis in the life science industry, Candish, L.; Collins, K. D.; Cook, G. C.; Douglas, J. J.; Gómez-Suárez, A.; Jolit, A.; Keess, S., *Chem. Rev.* **2022,** 122(2), 2907.
4. A small-footprint, high-capacity flow reactor for UV photochemical synthesis on the kilogram scale, Elliott, L. D.; Berry, M.; Harji, B.; Klauber, D.; Leonard, J.; Booker-Milburn, K. I., *Org. Process Res. Dev.* **2016,** 20(10), 1806.
5. Continuous-flow technology—a tool for the safe manufacturing of active pharmaceutical ingredients, Gutmann, B.; Cantillo, D.; Kappe, C. O., *Angew. Chem. Int. Ed.* **2015,** 54(23), 6688.
6. Design of a kilogram scale, plug flow photoreactor enabled by high power leds, Lévesque, F.; Di Maso, M. J.; Narsimhan, K.; Wismer, M. K.; Naber, J. R., *Org. Process Res. Dev.* **2020,** 24(12), 2935.
7. Integrated microfluidic reactors, Lin, W.-Y.; Wang, Y.; Wang, S.; Tseng, H.-R., *Nano Today* **2009,** 4(6), 470.
8. Scalable continuous vortex reactor for gram to kilo scale for UV and visible photochemistry, Lee, D. S.; Sharabi, M.; Jefferson-Loveday, R.; Pickering, S. J.; Poliakoff, M.; George, M. W., *Org. Process Res. Dev.* **2020,** 24(2), 201.
9. Why flow means green – evaluating the merits of continuous processing in the context of sustainability, Dallinger, D.; Kappe, C. O., *Curr. Opin. Green Sustain. Chem.* **2017,** 7, 6.
10. Flow chemistry: Recent developments in the synthesis of pharmaceutical products, Porta, R.; Benaglia, M.; Puglisi, A., *Org. Process Res. Dev.* **2016,** 20(1), 2.
11. Micromixers—a review on passive and active mixing principles, Hessel, V.; Löwe, H.; Schönfeld, F., *Chem. Eng. Sci.* **2005,** 60(8), 2479.
12. Continuous flow techniques in organic synthesis, Jas, G.; Kirschning, A., *Chemistry – A European Journal* **2003,** 9(23), 5708.
13. Flow photochemistry: Shine some light on those tubes!, Sambiagio, C.; Noël, T., *Trends Chem.* **2020,** 2(2), 92.
14. Heterogeneous catalysis under flow for the 21st century fine chemical industry, Ciriminna, R.; Pagliaro, M.; Luque, R., *Green Energy Environ.* **2021,** 6(2), 161.
15. The hitchhiker's guide to flow chemistry, Plutschack, M. B.; Pieber, B.; Gilmore, K.; Seeberger, P. H., *Chem. Rev.* **2017,** 117(18), 11796.
16. Heterogeneous photocatalysis in flow chemical reactors, Thomson, C. G.; Lee, A. L.; Vilela, F., *Beilstein J. Org. Chem.* **2020,** 16, 1495.
17. A fixed-bed photoreactor using conjugated nanoporous polymer-coated glass fibers for visible light-promoted continuous photoredox reactions, Huang, W.; Ma, B. C.; Wang, D.; Wang, Z. J.; Li, R.; Wang, L.; Landfester, K.; Zhang, K. A. I., *J. Mater. Chem. A* **2017,** 5(8), 3792.
18. A coating from nature, Hermens, J. G. H.; Freese, T.; van den Berg, K. J.; van Gemert, R.; Feringa, B. L., *Sci. Adv.* **2020,** 6(51), eabe0026.
19. Heterogeneous photoredox flow chemistry for the scalable organosynthesis of fine chemicals, Yang, C.; Li, R.; Zhang, K. A. I.; Lin, W.; Landfester, K.; Wang, X., *Nat. Comm.* **2020,** 11(1), 1239.
20. Scale-up of a heterogeneous photocatalytic degradation using a photochemical rotor–stator spinning disk reactor, Chaudhuri, A.; Zondag, S. D. A.; Schuurmans, J. H. A.; van der Schaaf, J.; Noël, T., *Org. Process Res. Dev.* **2022,** 26(4), 1279.
21. The E factor 25 years on: The rise of green chemistry and sustainability, Sheldon, R. A., *Green Chem.* **2017,** 19(1), 18.
22. Quid pro flow, Laybourn, A.; Robertson, K.; Slater, A. G., *J. Am. Chem. Soc.* **2023**.
23. Bayesian self-optimization for telescoped continuous flow synthesis, Clayton, A. D.; Pyzer-Knapp, E. O.; Purdie, M.; Jones, M. F.; Barthelme, A.; Pavey, J.; Kapur, N.; Chamberlain, T. W.; Blacker, A. J.; Bourne, R. A., *Angew. Chem. Int. Ed.* **2022**.
24. Glass wool: A novel support for heterogeneous catalysis, Elhage, A.; Wang, B. W.; Marina, N.; Marin, M. L.; Cruz, M.; Lanterna, A. E.; Scaiano, J. C., *Chem. Sci.* **2018,** 9(33), 6844.
25. Heterogeneous photoredox catalysis using fluorescein polymer brush functionalized glass beads, Bell, K.; Freeburne, S.; Fromel, M.; Oh, H. J.; Pester, C. W., *J. Polymer Sci.* **2021,** 59(22), 2844.
26. Performances of homogeneous and heterogenized methylene blue on silica under red light in batch and continuous flow photochemical reactors, Lancel, M.; Gomez, C.; Port, M.; Amara, Z., *Front. Chem. Eng.* **2021,** 3.
27. Heterogeneous photoredox catalysis based on silica mesoporous material and eosin Y: Impact of material support on selectivity of radical cyclization, Mahmoud, N.; Awassa, J.; Toufaily, J.; Lebeau, B.; Daou, T. J.; Cormier, M.; Goddard, J. P., *Molecules* **2023,** 28(2).
28. Outer-sphere effects in visible-light photochemical oxidations with immobilized and recyclable ruthenium bipyridyl salts, Tambosco, B.; Segura, K.; Seyrig, C.; Cabrera, D.; Port, M.; Ferroud, C.; Amara, Z., *ACS Catal.* **2018,** 8(5), 4383.
29. Organic/inorganic heterogeneous silica-based photoredox catalyst for aza-Henry reactions, Soria-Castro, S. M.; Lebeau, B.; Cormier, M.; Neunlist, S.; Daou, T. J.; Goddard, J.-P., *Eur. J. Org. Chem.* **2020,** 2020(10), 1572.
30. Perylene-grafted silicas: Mechanistic study and applications in heterogeneous photoredox catalysis, Carrillo, A. I.; Elhage, A.; Marin, M. L.; Lanterna, A. E., *Chem. Eur. J.* **2019,** 25(65), 14928.
31. Glass wool supported ruthenium complexes: Versatile, recyclable heterogeneous photoredox catalysts, Teixeira, R. I.; de Lucas, N. C.; Garden, S. J.; Lanterna, A. E.; Scaiano, J. C., *Cat. Sci. Tech.* **2020,** 10(5), 1273.
32. Nitro to amine reductions using aqueous flow catalysis under ambient conditions, Yaghmaei, M.; Lanterna, A. E.; Scaiano, J. C., *iScience* **2021,** 24(12).
33. Organic dyes supported on silicon-based materials: Synthesis and applications as photocatalysts, Mora-Rodríguez, S. E.; Camacho-Ramírez, A.; Cervantes-González, J.; Vázquez, M. A.; Cervantes-Jauregui, J. A.; Feliciano, A.; Guerra-Contreras, A.; Lagunas-Rivera, S., *Org. Chem. Front.* **2022,** 9(10), 2856.
34. Highly performing iodoperfluoroalkylation of alkenes triggered by the photochemical activity of perylene diimides, Rosso, C.; Filippini, G.; Cozzi, P. G.; Gualandi, A.; Prato, M., *ChemPhotoChem* **2019,** 3(4), 193.
35. Visible-light photocatalytic aerobic oxidation of sulfides to sulfoxides with a perylene diimide photocatalyst, Gao, Y.; Xu, H.; Zhang, S.; Zhang, Y.; Tang, C.; Fan, W., *Org. Biomolec. Chem.* **2019,** 17(30), 7144.
36. Mechanistic insights into two-photon-driven photocatalysis in organic synthesis, Marchini, M.; Gualandi, A.; Mengozzi, L.; Franchi, P.; Lucarini, M.; Cozzi, P. G.; Balzani, V.; Ceroni, P., *Phys. Chem. Chem. Phys.* **2018,** 20(12), 8071.
37. Organic photoredox catalysis, Romero, N. A.; Nicewicz, D. A., *Chem. Rev.* **2016,** 116(17), 10075.
38. Real roles of perylene diimides for improving photocatalytic activity, Zhang, F.; Li, W.; Jiang, T.; Li, X.; Shao, Y.; Ma, Y.; Wu, J., *RSC Adv.* **2020,** 10(39), 23024.
39. Cloud-inspired multiple scattering for light intensified photochemical flow reactors, Zheng, L.; Xue, H.; Wong, W. K.; Cao, H.; Wu, J.; Khan, S. A., *React. Chem. Eng.* **2020,** 5(6), 1058.

40. Mixing and enzyme reactions in a microchannel packed with glass beads, Sotowa, K. I.; Miyoshi, R.; Lee, C. G.; Kang, Y.; Kusakabe, K., *Korean J. Chem. Eng.* **2005,** 22(4), 552.
41. UV photovap: Demonstrating how a simple and versatile reactor based on a conventional rotary evaporator can be used for UV photochemistry, Clark, C. A.; Lee, D. S.; Pickering, S. J.; Poliakoff, M.; George, M. W., *Org. Process Res. Dev.* **2018,** 22(5), 595.
42. Safety assessment in development and operation of modular continuous-flow processes, Kockmann, N.; Thenée, P.; Fleischer-Trebes, C.; Laudadio, G.; Noël, T., *React. Chem. Eng.* **2017,** 2(3), 258.
43. Bimetallic magnetic PtPd-nanoparticles as efficient catalyst for PAH removal from liquid media, Zanato, A. F. S.; Silva, V. C.; Lima, D. A.; Jacinto, M. J., *Appl. Nanosci.* **2017,** 7(8), 781.
44. Preparation and characterization of magnetic photocatalyst from the banded iron formation for effective photodegradation of methylene blue under UV and visible illumination, Sanad, M. M. S.; Farahat, M. M.; El-Hout, S. I.; El-Sheikh, S. M., *J. Environ. Chem. Eng.* **2021,** 9(2), 105127.
45. A novel magnetic photocatalyst $Bi_3O_4Cl/SrFe_{12}O_{19}$: Fabrication, characterization and its photocatalytic activity, Wang, H.; Xu, L.; Liu, C.; Jiang, Z.; Feng, Q.; Wu, T.; Wang, R., *Ceram. Int.* **2020,** 46(1), 460.
46. Photocatalysis meets magnetism: Designing magnetically recoverable supports for visible-light photocatalysis, Terra, J. C. S.; Desgranges, A.; Monnereau, C.; Sanchez, E. H.; De Toro, J. A.; Amara, Z.; Moores, A., *ACS App. Mater. Inter.* **2020,** 12(22), 24895.
47. Porous phosphate-based glass microspheres show biocompatibility, tissue infiltration, and osteogenic onset in an ovine bone defect model, McLaren, J. S.; Macri-Pellizzeri, L.; Hossain, K. M. Z.; Patel, U.; Grant, D. M.; Scammell, B. E.; Ahmed, I.; Sottile, V., *ACS App. Mater. Inter.* **2019,** 11(17), 15436.
48. Fluid flow through packed columns, Ergun, S., *Chem. Eng. Prog.* **1952,** 48, 89.
49. Quantification and stability determination of surface amine groups on silica nanoparticles using solution nmr, Kunc, F.; Balhara, V.; Brinkmann, A.; Sun, Y.; Leek, D. M.; Johnston, L. J., *Anal. Chem.* **2018,** 90(22), 13322.
50. Use of perylene diimides in synthetic photochemistry, Rosso, C.; Filippini, G.; Prato, M., *Eur. J. Org. Chem.* **2021,** 2021(8), 1193.
51. Optimization of omeprazole synthesis: Physico-chemical steering towards greener processes, Vojčić, N.; Bregović, N.; Cindro, N.; Požar, J.; Horvat, G.; Pičuljan, K.; Meštrović, E.; Tomišić, V., *ChemistrySelect* **2017,** 2(17), 4899.
52. Photochemical aerobic oxidation of sulfides to sulfoxides: The crucial role of wavelength irradiation, Skolia, E.; Gkizis, P. L.; Nikitas, N. F.; Kokotos, C. G., *Green Chem.* **2022,** 24(10), 4108.
53. Oxidation of sulfides and disulfides under electron transfer or singlet oxygen photosensitization using soluble or grafted sensitizers, Lacombe, S.; Cardy, H.; Simon, M.; Khoukh, A.; Soumillion, J. P.; Ayadim, M., *Photochem. Photobiol. Sci.* **2002,** 1(5), 347.
54. Visible light sensitizer-catalyzed highly selective photo oxidation from thioethers into sulfoxides under aerobic condition, Ye, C.; Zhang, Y.; Ding, A.; Hu, Y.; Guo, H., *Sci. Rep.* **2018,** 8(1), 2205.
55. Solubility of oxygen in organic solvents and calculation of the hansen solubility parameters of oxygen, Sato, T.; Hamada, Y.; Sumikawa, M.; Araki, S.; Yamamoto, H., *Ind. Eng. Chem. Res.* **2014,** 53(49), 19331.